

# Atomic thermometry with modulation transfer spectroscopy of potassium D1 and D2 transitions

Cite as: J. Appl. Phys. 138, 064401 (2025); doi: 10.1063/5.0280709

Submitted: 14 May 2025 · Accepted: 18 July 2025 ·

Published Online: 8 August 2025



View Online



Export Citation



CrossMark

Prosenjit Majumder<sup>1,2,a)</sup> 

## AFFILIATIONS

<sup>1</sup>Photonics Laboratory, Physics Unit, Tampere University, Tampere 33720, Finland

<sup>2</sup>Department of Physics, Durham University, South Road, Durham DH1 3LE, United Kingdom

<sup>a)</sup>Author to whom correspondence should be addressed: [prosenjit.majumder@tuni.fi](mailto:prosenjit.majumder@tuni.fi)

## ABSTRACT

We report on temperature study of modulation transfer spectroscopy of the  $4S_{1/2} \rightarrow 4P_{1/2}$  (D1) and  $4S_{1/2} \rightarrow 4P_{3/2}$  (D2) transition of naturally abundant potassium in a vapor cell. This transition is critical for laser cooling and optical pumping of potassium and for robust laser frequency stabilization. However, no prior work has explored their use as atomic thermometers. Our study is, therefore, motivated us to consider D1 and D2 transitions as a atomic thermometry. Interestingly, despite the absence of a closed transition, the small ground-state hyperfine splitting in potassium results in strong crossover features in the D1 modulation transfer spectrum. To emphasize this, we compare the temperature dependency of D1 and D2 spectra of potassium. Further, we compare our experimental results of different pump-probe polarization configurations to identify the optimal signals for modulation transfer spectrum. We find nice zero crossing for different polarization configurations and compare the sensitivity.

© 2025 Author(s). All article content, except where otherwise noted, is licensed under a Creative Commons Attribution (CC BY) license (<https://creativecommons.org/licenses/by/4.0/>). <https://doi.org/10.1063/5.0280709>

## I. INTRODUCTION

Spectroscopy has long been a fundamental tool in atomic physics, providing crucial insights into atomic structures and enabling precision measurements that have significantly advanced fields such as quantum optics, metrology, and laser-based cooling techniques. Its applications range from laser cooling and trapping of neutral atoms<sup>1</sup> and molecules<sup>2,3</sup> to optical pumping<sup>4</sup> and high-precision frequency stabilization.<sup>5,6</sup> For alkali-metal atoms, achieving laser frequency stability on the order of  $\approx$  MHz is essential for many precision experiments and quantum technologies. One widely adopted approach for maintaining such stability involves using atomic spectroscopy to extract an error signal from an atomic transition, which is then utilized in a feedback loop to correct frequency deviations of the laser.

In this work, we investigate the use of modulation transfer spectroscopy (MTS)<sup>5,7–9</sup> not only as a tool for frequency stabilization but also as a potential method for atomic thermometry. Specifically, we focus on the D1 ( $4S_{1/2} \rightarrow 4P_{1/2}$ ) and D2 ( $4S_{1/2} \rightarrow 4P_{3/2}$ ) transitions in naturally abundant potassium vapor. While these transitions have been extensively studied for their roles in laser cooling, repump, and frequency stabilization, their

dependence on atomic temperature and potential use as a thermometer remain largely unexplored. Our study aims to fill this gap by examining the temperature-dependent behavior of the MTS signals for these transitions. MTS is a well-established pump-probe spectroscopy technique that exploits nonlinear optical effects to generate highly sensitive spectroscopic signals. In this method, an electro-optic modulator (EOM) is used to modulate the frequency of the pump beam, creating sidebands along with the carrier frequency. When this modulated pump beam is spatially overlapped with a probe beam in an atomic vapor cell and tuned near an atomic transition, where a four-wave mixing process takes place.<sup>10</sup> This process transfers the sidebands from the pump to the probe, producing interference patterns that can be detected by a fast photodiode. By demodulating this photodiode signal, the MTS signal is extracted, yielding a high-contrast dispersive spectral feature.

The MTS offers two key advantages that make it a powerful tool for precision spectroscopy. First, MTS generates a dispersive signal with a well-defined zero crossing on a flat background, which is ideal for high-precision laser frequency monitoring. The zero crossing corresponds precisely to the resonance condition, enabling accurate detection of frequency fluctuations caused by

25 August 2025 08:50:43

external perturbations. This feature is particularly valuable in applications requiring stable laser frequencies, such as atomic clocks, quantum computing, and precision metrology. Second, while MTS signals are primarily influenced by cycling transitions, they also provide insights into non-cycling transitions.<sup>5</sup> This capability is especially beneficial in systems with narrow hyperfine structures that are difficult to resolve using conventional spectroscopic techniques. For example, in potassium, the  $4S_{1/2} \rightarrow 4P_{1/2}$  (D1) transition in bosonic isotopes exhibits closely spaced hyperfine levels that are challenging to distinguish with Doppler-free saturation spectroscopy.<sup>11</sup> MTS, however, can resolve these fine structures, making it a superior choice for studying such systems.

A unique aspect of potassium spectroscopy is the presence of strong crossover resonances in the D1 transition, which arise from the relatively small hyperfine splitting in the ground state. These crossover features are highly sensitive to temperature variations within the vapor cell, making the D1 transition a promising candidate for atomic thermometry. In contrast, the D2 line features a dominant cycling transition that efficiently optically pumps atoms into a stretched Zeeman sublevel (e.g.,  $F = 2$ ,  $m_F = 2$ ). Once atoms accumulate in this state, they are no longer effectively coupled into the crossover configuration, and D2 excited state has four hyperfine levels, leading to more decay channels and less efficient sideband transfer in the four-wave mixing process required for MTS, which significantly reduces the modulation transfer signal associated with crossover features. As a result, the D2 transition exhibits weaker crossover signatures and a distinct, more stable response to temperature variations compared to the D1 line. By systematically analyzing the temperature-dependent behavior of these transitions, we explore the feasibility of using atomic transitions as a precise tool for temperature measurement. This dual capability of MTS—enabling both high-precision frequency stabilization and temperature sensing—highlights its versatility and potential for advancing applications in atomic physics, quantum optics, and precision metrology. The ability to resolve fine spectral features and monitor temperature-dependent changes in atomic transitions opens new avenues for research and technological innovation.

Modulation transfer spectroscopy (MTS) has emerged as a powerful technique for laser frequency stabilization and high-resolution spectroscopy. However, its potential application in atomic thermometry remains relatively underexplored. In this work, we investigate the temperature dependence of the D1 and D2 transitions in potassium vapor and demonstrate how MTS can function not only as a precise frequency reference but also as a sensitive thermometer for atomic systems.

The D1 line, lacking a closed cycling transition, is particularly prone to optical pumping effects and population redistribution as the temperature and consequently the vapor density increases. This leads to pronounced distortion and variation in the MTS signal. A key feature of the D1 line is the presence of a strong ground-state crossover transition, which behaves almost like a closed transition but exhibits high sensitivity to optical depth and, therefore, to temperature. As a result, the D1 signal shows significant temperature induced changes in both amplitude and shape. In contrast, the D2 line includes a nearly closed cycling transition  $F = 2 \rightarrow F' = 1, 2$ ,

which effectively confines atoms within a stable excitation loop. This configuration reduces the impact of optical pumping, suppresses crossover features, and leads to greater spectral stability with respect to temperature variations. While the D1 transition offers strong temperature sensitivity due to its hyperfine structure and population dynamics, the D2 transition provides enhanced spectral robustness, making it a more stable reference in temperature-variable environments. These complementary characteristics highlight the dual utility of MTS for accurate frequency locking and for real time thermometric diagnostics in atomic vapors.

Our findings open new avenues for implementing MTS-based thermometry in various atomic systems, with potential applications in precision metrology, atomic clocks, and quantum sensing. By refining this approach and extending it to other atomic species, this study lays the groundwork for advanced spectroscopic techniques in both fundamental research and applied physics.

## II. THEORETICAL BACKGROUND

For a weak non-saturating probe, the transmitted signal normalized to the incident intensity is described by the exponential decay  $\exp(-\alpha)$ , where  $\alpha$  represents the absorption coefficient. In a two-level atomic system, the introduction of a saturating beam induces a Lamb dip in the probe absorption coefficient.<sup>12,13</sup> This phenomenon can be mathematically expressed as

$$\alpha_S = \alpha_D(1 - L), \quad (1)$$

where  $\alpha_D$  denotes the Doppler-broadened absorption coefficient and  $L = \frac{a}{1 + \delta^2/\gamma^2}$  is a Lorentzian function that depends on the detuning  $\delta$  from the Doppler-free resonance. The amplitude and width of  $L$  are influenced by the intensity of the pump beam. Given that  $\alpha_D$  is proportional to the vapor pressure  $P_{\text{vap}}$ , we can express it as  $\alpha_D = a_G P_{\text{vap}}$ . The difference in transmission with and without the saturating beam is then given by

$$\Delta S = e^{-a_G P_{\text{vap}}(T)} \left( e^{a_I a_G P_{\text{vap}}(T)/(1 + \delta^2/\gamma^2)} - 1 \right). \quad (2)$$

By incorporating the temperature dependence of vapor pressure from Refs. 14–16, we model the relationship as

$$P_{\text{vap}}(T) = e^{aT^3 + bT^2 + cT + d}, \quad (3)$$

where  $T$  is the temperature in Kelvin and  $a$ ,  $b$ ,  $c$ , and  $d$  are empirically determined coefficients.<sup>14</sup> This formulation allows for a detailed analysis of the temperature effects on  $\Delta S$ , which has been evaluated and modeled in Figs. 3(a) and 3(b). The relationship between temperature and the signal variation provides a robust framework for understanding how thermal changes influence atomic transitions, making it a valuable tool for precision thermometry.

The temperature-dependent signal variation ( $\Delta S$ ) for the D1 (770 nm) and D2 (767 nm) atomic transitions was modeled using a combined framework of vapor pressure dynamics and Lorentzian response. The detuning  $\delta$ , along with transition-specific parameters

such as the gain coefficient  $a_G$ , saturation factor  $a_L$ , and linewidth  $\gamma$ , play a critical role in shaping the signal. For the D1 transitions, three cases were examined ( $a_G = 200, 100, 75$ ;  $\delta = 10.0, 15.8, 11.7$  MHz), while two D2 transitions ( $a_G = 500, 300$ ;  $\delta = 10.0, 15.8$  MHz) were simulated over a temperature range of 27–127 °C, as presented in Figs. 3(a) and 3(b). The normalized  $\Delta S$  curves, scaled to the peak value of transition 1, revealed distinct thermal optima. Experimental data were also presented, showing qualitative agreement with theoretical predictions as shown in Figs. 3(a) and 3(c). Higher values of  $a_G$  (e.g., 500 for D2) led to a suppression of  $\Delta S$  at elevated temperatures due to stronger damping driven by vapor pressure. Conversely, increased detuning (e.g.,  $\delta = 15.8$  MHz) resulted in a broadening and redshift of the Lorentzian response. These findings underscore the intricate interplay between thermal vapor dynamics and resonant detuning, which is crucial for optimizing atomic transition signals in applications such as laser spectroscopy based sensors.

### A. Atomic transitions in potassium

Potassium (K) has a ground-state configuration of  $4S_{1/2}$ , with two excited states,  $4P_{1/2}$  (D1) and  $4P_{3/2}$  (D2). The hyperfine splitting of the ground state ( $F = 1$  and  $F = 2$ ) is relatively small (462 MHz for  $^{39}\text{K}$ ), leading to significant overlap between the hyperfine levels in the D1 transition. This results in strong crossover resonances, which are sensitive to temperature changes due to the population distribution among the hyperfine levels.

On the other hand, the D2 transition has a smaller multiple hyperfine splitting in the excited state and has a dominating cycling transition that quickly pumps atoms into a stretched state, leading to weaker crossover features, as presented in Fig. 1. The temperature dependence of these transitions can be modeled using the Boltzmann distribution, which describes the population of atomic states as a function of temperature. We also analyze four polarization configurations for the counter-propagating pump and probe laser beams: (i)  $lin \parallel lin$ , (ii)  $lin \perp lin$ , (iii)  $\sigma^+ - \sigma^+$ , and (iv)  $\sigma^+ - \sigma^-$ . For simplicity, the circularly polarized cases (iii) and (iv) are labeled according to the transitions they drive. In the linear polarization configurations, the quantization axis is defined along the electric field direction of the pump beam, whereas for circular polarization configurations, the pump beam's propagation direction serves as the quantization axis. To maintain a well-defined quantization axis in the experiment, we apply a weak magnetic field parallel to the beam propagation direction.

### B. MTS spectrum theory

To analyze the internal atomic dynamics, the density matrix equation is solved as<sup>5,8,19–21</sup>

$$\dot{\rho} = -\frac{i}{\hbar}[H_0 + V, \rho] + \dot{\rho}_{\text{relax}}, \quad (4)$$

where  $\rho$  is the density operator,  $H_0$  the atomic Hamiltonian, and  $V$  the atom-field interaction.  $\dot{\rho}_{\text{relax}}$  accounts for relaxation effects such as spontaneous emission and transit time decay.<sup>8,19,22</sup>

The atomic Hamiltonian  $H_0$  includes detuning  $\delta_1$ , ground- and excited-state splittings  $\Delta_g$  and  $\Delta_e$ , and excludes magnetic-field

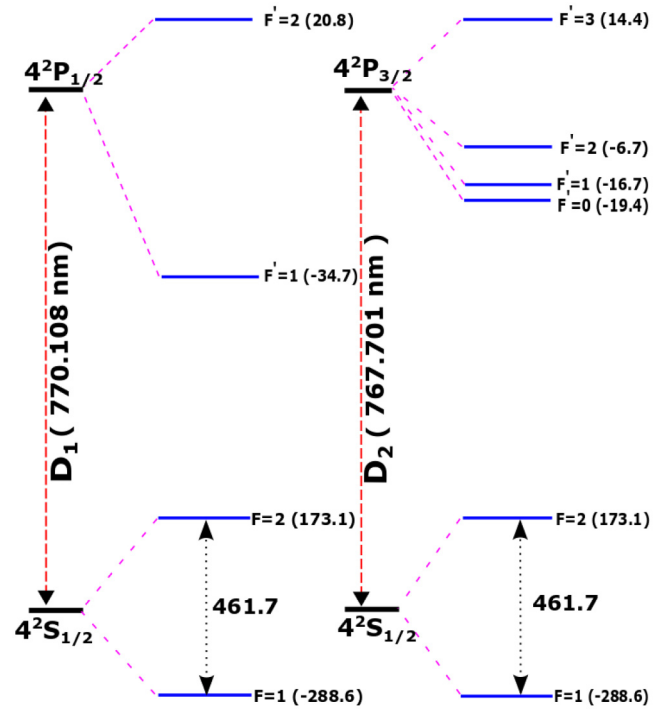


FIG. 1. Hyperfine structure of potassium for the D1 and D2 transitions. The energy levels are labeled by the total angular momentum quantum number  $F$ , with hyperfine shifts given in MHz based on values from Refs. 17 and 18. The relative transition frequencies are highlighted, illustrating the differences in hyperfine splitting between the two transitions.

25 August 2025 08:50:43

effects,

$$H_0 = -\sum_{m'=-2}^2 \hbar \delta_1 |F' = 2, m'\rangle \langle F' = 2, m'| - \sum_{m'=-1}^1 \hbar (\delta_1 + \Delta_e) |F' = 1, m'\rangle \langle F' = 1, m'| - \sum_{m=-1}^1 \hbar \Delta_g |F = 1, m\rangle \langle F = 1, m|. \quad (5)$$

The interaction Hamiltonian  $V$  captures the coupling between atomic states and the probe and modulated pump beams,

$$V = \sum_{F=1}^2 \sum_{F'=1}^2 \sum_{m=-F}^F \sum_{q=\pm,0} \frac{\hbar}{2} [c_q \Omega_p e^{-i\delta_p t} + a_q (\Omega_c + \Omega_s e^{-i\Omega t} - \Omega_s e^{i\Omega t})] C_{F,m}^{F',m+q} |F', m+q\rangle \langle F, m| + \text{h.c.} \quad (6)$$

Here,  $\delta_1 = \delta + kv$ ,  $\delta_p = -2kv$ , and  $C_{F,m}^{F',m'}$  are Clebsch-Gordan coefficients.  $\Omega_p$ ,  $\Omega_c$ , and  $\Omega_s$  are the Rabi frequencies of the

probe and pump components, and  $c_q$ ,  $a_q$  are the electric field coefficients in the spherical basis.

By expanding the density matrix, we derive a system of coupled differential equations, solved in steady state for each velocity class  $v$ . The modulation transfer spectroscopy (MTS) signal is extracted from the optical coherences at frequencies  $-\delta_p \pm \Omega$ , with in-phase and quadrature components given by

$$I_n = \sum_{F=1}^2 \sum_{F'=1}^2 \sum_{m=-F}^F \sum_{q=\pm,0} c_q C_{F,m}^{F',m+q} \int_{-\infty}^{\infty} dv f_D(v) \times \left( s_{F,m}^{F',m+q(-)} + s_{F,m}^{F',m+q(+)} \right), \quad (7)$$

$$Q_n = \sum_{F=1}^2 \sum_{F'=1}^2 \sum_{m=-F}^F \sum_{q=\pm,0} c_q C_{F,m}^{F',m+q} \int_{-\infty}^{\infty} dv f_D(v) \times \left( -r_{F,m}^{F',m+q(-)} + r_{F,m}^{F',m+q(+)} \right), \quad (8)$$

where  $f_D(v)$  is the Maxwell-Boltzmann distribution,

$$f_D(v) = \frac{1}{\sqrt{\pi}u} e^{-\left(\frac{v}{u}\right)^2}. \quad (9)$$

Total MTS signals from both isotopes ( $^{39}\text{K}$  and  $^{41}\text{K}$ ) are combined as

$$I(\delta) = \frac{N_{39}}{N_{39} + N_{41}} I_{39}(\delta) + \frac{N_{41}}{N_{39} + N_{41}} I_{41}(\delta - \Delta), \quad (10)$$

$$Q(\delta) = \frac{N_{39}}{N_{39} + N_{41}} Q_{39}(\delta) + \frac{N_{41}}{N_{39} + N_{41}} Q_{41}(\delta - \Delta), \quad (11)$$

with  $\Delta = 2\pi \times 305$  MHz denoting the isotope shift.

The total experimental signal is expressed as

$$S[\delta, \phi] = A(I(\delta) \cos \tilde{\phi} + Q(\delta) \sin \tilde{\phi}), \quad (12)$$

where  $\tilde{\phi} = \phi - \phi_0$  accounts for the phase set by the AFG and an experimental offset  $\phi_0$ , which is greatly agreed with our previous data.<sup>5</sup>

### III. EXPERIMENTAL SETUP

A home-built narrow-linewidth external cavity diode laser serves as the light source. The laser output is coupled into a single-mode, polarization-maintaining optical fiber to ensure a gaussian beam profile at the output. To regulate the total optical power delivered to the spectroscopy setup and to adjust the power ratio between the pump and probe beams, a combination of two polarizing beam splitters (PBS) and a pair of half-wave plates ( $\lambda/2$ ) and quarter-waveplate ( $\lambda/4$ ) are employed.

The probe beam is directed into a 2 cm long potassium vapor cell. The cell is enclosed within a brass housing equipped with heating elements to control its temperature. The temperature is stabilized at  $99 \pm 2^\circ\text{C}$ , corresponding to an estimated vapor pressure of  $3.5 \times 10^{-5}$  mbar. Both the pump and probe beams are

collimated, with their  $1/e^2$  diameters at the center of the vapor cell measured to be  $2.06 \pm 0.02$  and  $1.96 \pm 0.05$  mm, respectively. To study the temperature dependence of the modulation transfer spectra, we constructed a home-built heating bath capable of maintaining a stable temperature for the potassium vapor cell. The heating bath consists of a temperature-controlled enclosure with a precision thermometer to monitor the temperature. The potassium vapor cell is placed inside this enclosure, and the temperature is varied systematically from 30 to  $140^\circ\text{C}$ .

To achieve optimal experimental conditions, we systematically optimized the intensities of the pump and probe beams. Initially, the pump intensity was optimized while maintaining a constant probe intensity of  $49.7 \pm 0.8$  mW/cm<sup>2</sup>. Subsequently, the probe intensity was optimized with the pump intensity fixed at  $35.5 \pm 0.2$  mW/cm<sup>2</sup>, a value chosen arbitrarily as a starting point. Through this iterative process, the optimal intensities were determined to be  $36 \pm 3$  mW/cm<sup>2</sup> for the pump beam and  $59.5 \pm 1.1$  mW/cm<sup>2</sup> for the probe beam. It is worth noting that the saturation intensity for the system is  $1.75$  mW/cm<sup>2</sup>, which is significantly lower than the optimized intensities used in the experiment.

The pump beam is modulated using a custom-built electro-optic modulator (EOM). The EOM consists of a LiTaO<sub>3</sub> crystal placed between two electrically connected brass capacitor (C) plates. By incorporating an inductor (L), the setup forms a simple LC circuit that enhances the voltage across the crystal through resonant amplification. The resonance frequency of the EOM is measured to be  $6.054 \pm 0.005$  MHz. The EOM is driven at this resonance with its maximum applied voltage, generating optical sidebands, each carrying  $15 \pm 1\%$  of the total pump beam intensity. Additional details regarding the EOM design and operation can be found in previous studies.<sup>23</sup>

We explore various configurations of laser polarization to analyze their effects on the measurement. To ensure a well-defined quantization axis, a weak magnetic field is applied using a set of rectangular coils that are concentric with the vapor cell. These coils generate a magnetic field of 1.5 G along the beam propagation axis at the center of the cell. By adjusting the waveplates, as indicated in Fig. 2(b), we investigate four distinct polarization configurations of the laser light passing through the cell: circular polarization where the pump and probe address opposite transitions ( $\sigma^+ - \sigma^-$ ), circular polarization where both drive the same transitions ( $\sigma^+ - \sigma^+$ ), linear polarization with mutually perpendicular pump and probe beams ( $lin \perp lin$ ), and linear polarization where they are parallel ( $lin \parallel lin$ ).

A phase-sensitive detection technique is employed using a simple electronic setup to demodulate the modulated transfer spectroscopy signal, as highlighted in faint green color. A custom-built high-speed photodiode detects the beat signal between the modulated probe carrier and its sidebands. This signal is processed through a bias-tee (Mini-Circuits model: ZFBT-4R2GW), which filters out the DC component corresponding to the standard saturated absorption profile and routes it to a secondary oscilloscope channel. The modulated component is then sent to a double-balanced mixer (DBM) (Mini-Circuits model: ZAD1H+), where it is multiplied with a reference signal generated by an arbitrary function generator (AFG) (Tektronix model: AFG 3102). The AFG

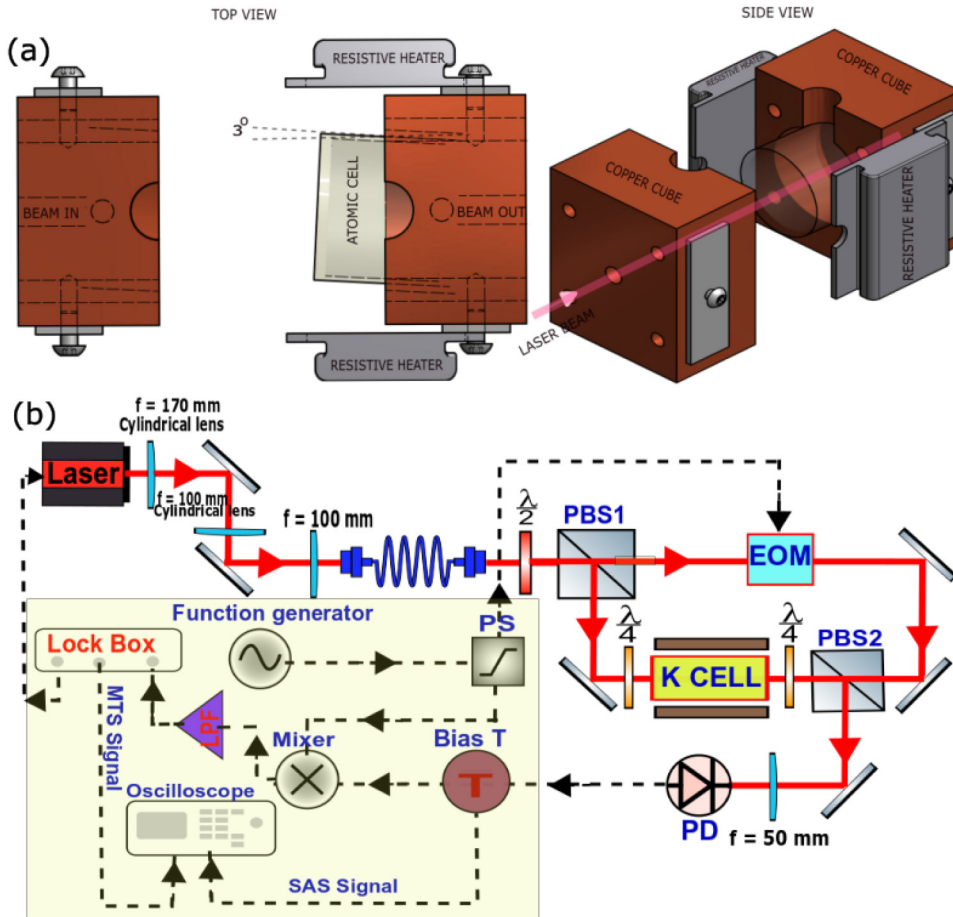


**FIG. 2.** (a) Schematic representation of the atomic vapor cell heating setup. The top and side views illustrate the positioning of the resistive heaters and copper cube surrounding the atomic cell. The laser beam propagates through the cell, allowing interaction with the atomic medium. The 3D view provides a clearer perspective on the setup, showing the placement of the optical path, heating elements, and the atomic vapor cell placed at an angle of  $3^\circ$  to eliminate beam reflections from the input and output surfaces. (b) Experimental setup for MTS experiment. A laser beam passes through a series of optical elements, including cylindrical lenses for beam shaping, polarization beam splitters (PBS1 and PBS2), and an electro-optic modulator (EOM) for frequency modulation. The potassium (K) atomic vapor cell is placed within the optical path, and the transmitted signal is detected by a photodiode (PD). The modulation and detection electronics include a function generator, lock-in detection components (lock box, mixer, bias T), and an oscilloscope for signal analysis, highlighted with a faint color.

25 August 2025 08:50:43

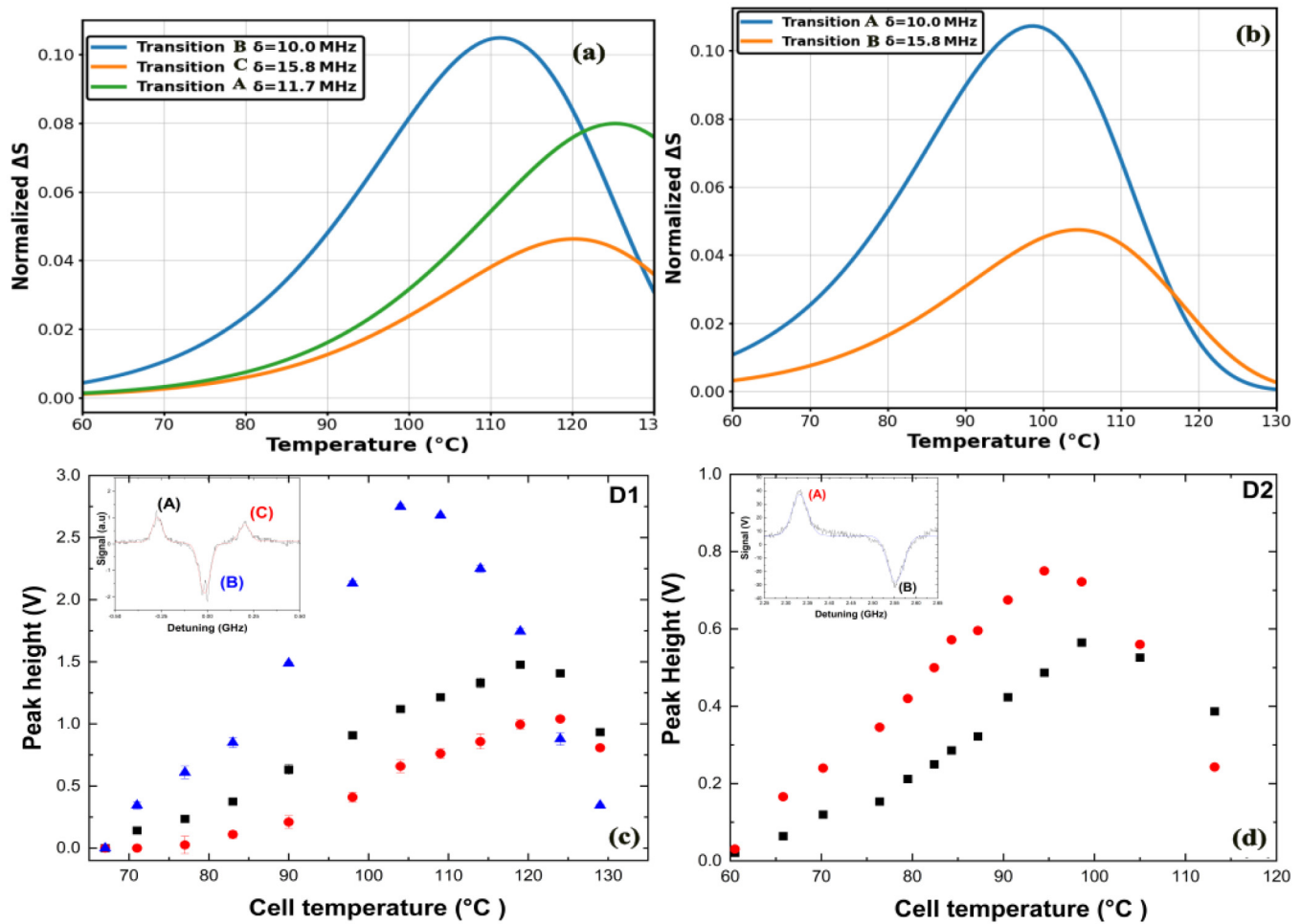
provides two outputs: one drives the electro-optic modulator (EOM), while the other serves as a local oscillator for reference in the demodulation process. The relative phase between these two outputs can be adjusted using the AFG, enabling precise characterization of the phase parameter. The transmitted signal detected by a fast photodiode with photosensitivity of 0.55 A/w. The demodulated signal is subsequently directed either to an oscilloscope for data acquisition or to a feedback loop for stabilizing the laser frequency.

#### IV. RESULTS AND DISCUSSION

In our modulation transfer spectroscopy experiment, two counter-propagating pump and probe beams interact within a potassium vapor cell. Due to the low number density and vapor pressure of potassium at room temperature, the cell is heated using a resistive heater, and the temperature is monitored with a thermistor. A photodetector captures the probe beam, which provides the MTS and saturation absorption spectroscopy (SAS) spectra, including the Doppler background, as shown in Figs. 3(c) and 3(d) also compare with the theoretical model. The spectrum reveals three prominent Lamb dips labeled A, B, and C for D1 transition. Here,

dip A corresponds to the  $F = 2 \rightarrow F' = 1, 2$  transition, dip B represents a crossover peak  $F = [1 \leftrightarrow 2] \rightarrow F' = 1, 2, 3$ , and dip C corresponds to the  $F = 1 \rightarrow F' = 2$  transition. The contributions of the  $^{40}\text{K}$  and  $^{41}\text{K}$  isotopes are negligible in the spectrum due to their low natural abundances. For the D2 transition in Fig. 3(d), the spectrum exhibits two main features, A and B, each comprising a group of overlapping transitions. Feature A corresponds to the  $F = 2 \rightarrow F' = 1, 2, 3$  transition, including crossover resonances within the excited states. Feature B consists of two ground-state crossover peaks  $F = [1 \leftrightarrow 2] \rightarrow F' = 1, 2, 3$  associated with actual transitions. The Doppler background of the saturation absorption spectrum is strongly influenced by temperature due to the exponential dependence of vapor pressure.

For the D1 transition, the Lamb dips begin to appear at  $70^\circ\text{C}$  and vanish beyond  $130^\circ\text{C}$ , as the cell becomes optically thick on resonance. The maximum Lamb dip for feature B occurs at  $104 \pm 3^\circ\text{C}$ , while features A and C exhibit optimal temperatures higher than that of B. For the D2 transition, peaks A and B become visible at  $65^\circ\text{C}$ , corresponding to the  $F = 2 \rightarrow F' = 1, 2, 3$  transition and the crossover  $F = [1 \leftrightarrow 2] \rightarrow F' = 1, 2, 3$  transition, respectively. We assume a small dip near 260 MHz is also observed, corresponding to the  $F = 1 \rightarrow F' = 0, 1, 2$  transition of  $^{39}\text{K}$ , which



25 August 2025 08:50:43

**FIG. 3.** Temperature dependence of Doppler-free SAS spectrum for different atomic transitions. Top row: Theoretical model showing normalized signal change ( $\Delta S$ ) as a function of temperature for selected transitions in the  $D_1$  (770 nm) and  $D_2$  (767 nm) lines. (a)  $D_1$  transitions exhibit distinct temperature-dependent behavior, with peak signals shifting and varying in intensity for different transitions. (b)  $D_2$  transitions demonstrate a non-linear dependence on temperature, with peak response occurring in an optimal temperature range. Bottom row: Experimental data showing peak height variations as a function of cell temperature. (c) Peak height measurements for the  $D_1$  transition, where different symbols represent distinct frequency components. The inset provides an example of the spectral features under study. (d) Temperature dependence of peak height for the  $D_2$  transition, showing an initial increase with temperature before reaching a maximum and subsequently declining.

overlaps with the  $^{41}\text{K}$  ground-state crossover, as shown in Fig. 5. The peaks disappear beyond  $115^\circ\text{C}$  due to the cell becoming optically thick. Both peaks A and B reach their maximum intensity at  $96 \pm 2^\circ\text{C}$ . To optimize the temperature dependence, both Doppler and sub-Doppler spectra were recorded at the same temperature within a short time window. By subtracting these two signals, a flat background with narrow features A and B is obtained, as illustrated in Figs. 3(c) and 3(d). A Lorentzian function was fitted to the data to extract the peak heights (amplitudes). The MTS spectrum primarily appears in the B peak of the  $D_1$  crossover transition. The intensity of the weak probe light propagating through the thermal cell, modulated by the Doppler profile, can be modeled using Eq. (3) and is presented in Figs. 3(a) and 3(b).

In both theoretical and experimental investigations, the temperature dependence of the amplitudes of peaks A, B, and C for the  $D_1$  (770.1 nm) and  $D_2$  (767.7 nm) transitions showed qualitative agreement. The observed discrepancies between the two approaches may stem from an imperfect knowledge of beam parameters, residual systematic effects, or differences arising from isotope shifts that are not fully accounted for in the model. For both transitions, the peak amplitudes increase with temperature, reaching their respective maxima at  $104 \pm 3^\circ\text{C}$  for the  $D_1$  transition and  $96 \pm 2^\circ\text{C}$  for the  $D_2$  transition. These temperatures correspond to optimal conditions for modulation transfer spectroscopy, beyond which the potassium vapor becomes optically thick. In this regime, the absorption increases significantly,

reducing the amount of transmitted light and thereby diminishing the overall signal strength.

Specifically, features B and C of the D1 transition, as well as feature B of the D2 transition, exhibit a clear decline in amplitude at elevated temperatures. This behavior reflects the transition from an absorption-limited regime to one where excessive optical density suppresses the contrast and clarity of spectral features. Understanding this thermal behavior is crucial for optimizing experimental conditions and achieving high-resolution spectroscopic measurements.

### A. Polarization configurations

By reconfiguring the waveplates, we can examine the modulation transfer spectroscopy signal for various polarization configurations. For D1 and D2, transitions are presented in Fig. 4. These measurements were taken with a phase  $\phi = 117.5^\circ$ , which is close to the optimal phase.<sup>5</sup> The laser parameters were maintained at the optimal values identified for the linear parallel (*lin* || *lin*) configuration. In the linear perpendicular (*lin*  $\perp$  *lin*) configuration, we observed a significant increase in the amplitude of the  $F = (1 \leftrightarrow 2) \rightarrow F' = 2$  signal and a reduction in the neighboring features. The experimental results also show for all configurations including for the  $\sigma^+ - \sigma^+$  case. For this configuration, the theory predicts broader features than those observed experimentally.<sup>5</sup> The Rabi frequencies of the laser beams in the experiment ranged between  $2\Gamma$  and  $4\Gamma$ . At these laser intensities, our assumption of three-photon interactions may be insufficient, particularly for the  $\sigma^+ - \sigma^+$  polarization configuration.

We examine four separate combinations of pump and probe beams, such as linear polarization defined as *lin*  $\perp$  *lin*, *lin* || *lin*,

and circular polarization defined as  $\sigma^+ - \sigma^+$  and  $\sigma^+ - \sigma^-$ , which can be obtained by rotating  $\lambda/2$  or  $\lambda/4$  waveplates on each end of the thermal cell, as shown in Fig. 4. In our experiment, the *lin*  $\perp$  *lin* and *lin* || *lin* combinations can be achieved by including the half-waveplates from each side of the vapor cell and arranging the proper angles of the half-waveplates to make the *lin*  $\perp$  *lin* and *lin* || *lin* polarization configurations. Then, we re-inserted the  $\lambda/4$  waveplates and removed the  $\lambda/2$  waveplates. The quarter-waveplates are then rotated to provide the correct polarization configuration for  $\sigma^+ - \sigma^+$  and  $\sigma^+ - \sigma^-$ . The results for the different configurations for both D1 and D2 transitions respectively, which are also comparable with our theoretical study. There is a significant role of the carrier, sidebands, and the probe frequencies, as indicated.<sup>5</sup>

The MTS spectrum for different polarization configurations is created by a coherent four-wave mixing process as indicated by Refs. 8, 19, and 24. As explained in Refs. 8 and 19, a long interaction leads to small amplitude and slope for crossover transition due to leakage of the population to the other states than unique ground states. In cycling transition, the big spectrum (in terms of amplitude) depends positively on the atom-light interaction time, i.e., higher signal for higher interaction time. In every plot, the phase angle indicates our phase is really a relative phase, for example, the zero phase in theory might not be zero for the experiments.

In Fig. 4(a) for the D1 line, we can see the amplitude and slope of crossover peaks for the  $F = [1 \leftrightarrow 2] \rightarrow F' = 2$  transition are maximum compared to other transitions and crossovers. In the four polarization configurations, the *lin* || *lin* configuration is smaller than the *lin*  $\perp$  *lin* configuration. While in the case of the  $\sigma^+ - \sigma^-$  polarization configuration, the amplitude is lower than the  $\sigma^+ - \sigma^+$  configuration. Similarly, in Fig. 4(b) for the D2 line, the maximum amplitude and slope are observed in the resonance

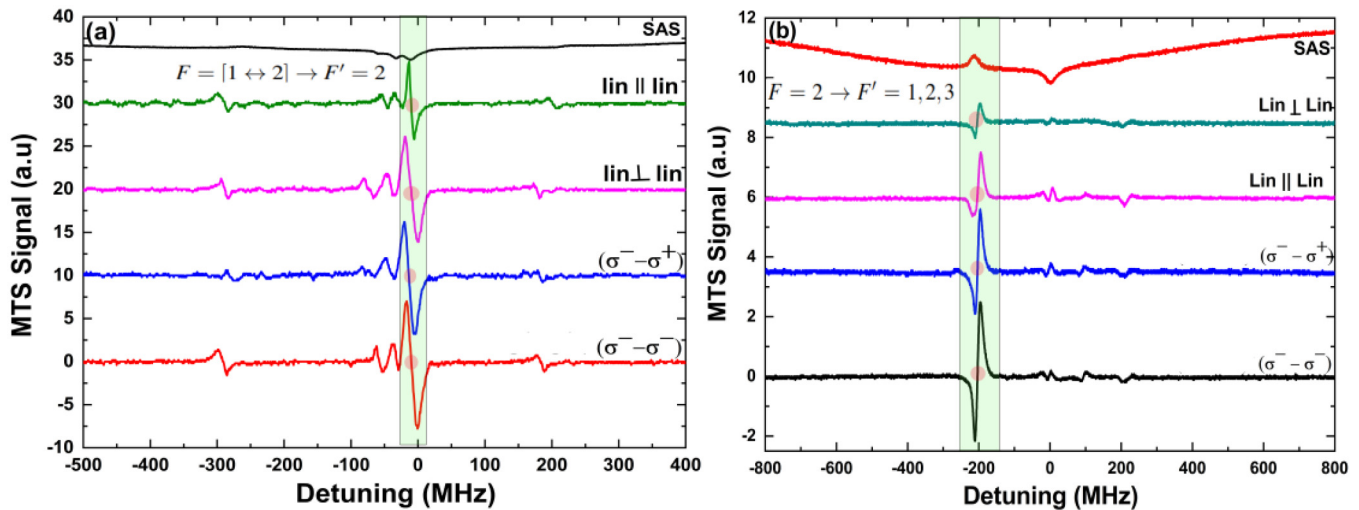


FIG. 4. The figure presents the MTS spectrum for different polarization configurations as a function of detuning. The spectra are obtained for various polarization states of the pump and probe beams, including linear-linear (*Lin* || *Lin*), linear-perpendicular (*Lin*  $\perp$  *Lin*), and circularly polarized configurations ( $\sigma^+ - \sigma^-$  and  $\sigma^- - \sigma^+$ ). The topmost trace represents the SAS signal for reference. The amplitude and shape of the MTS signals vary significantly depending on the polarization state, reflecting the influence of atomic selection rules and optical pumping effects on the spectroscopic response. (a) and (b) correspond to the D1 and D2 transitions, respectively, with the faint green color highlighting the transition of interest for this study. And, a faint red circle indicate the zero-crossing point.

25 August 2025 08:50:43

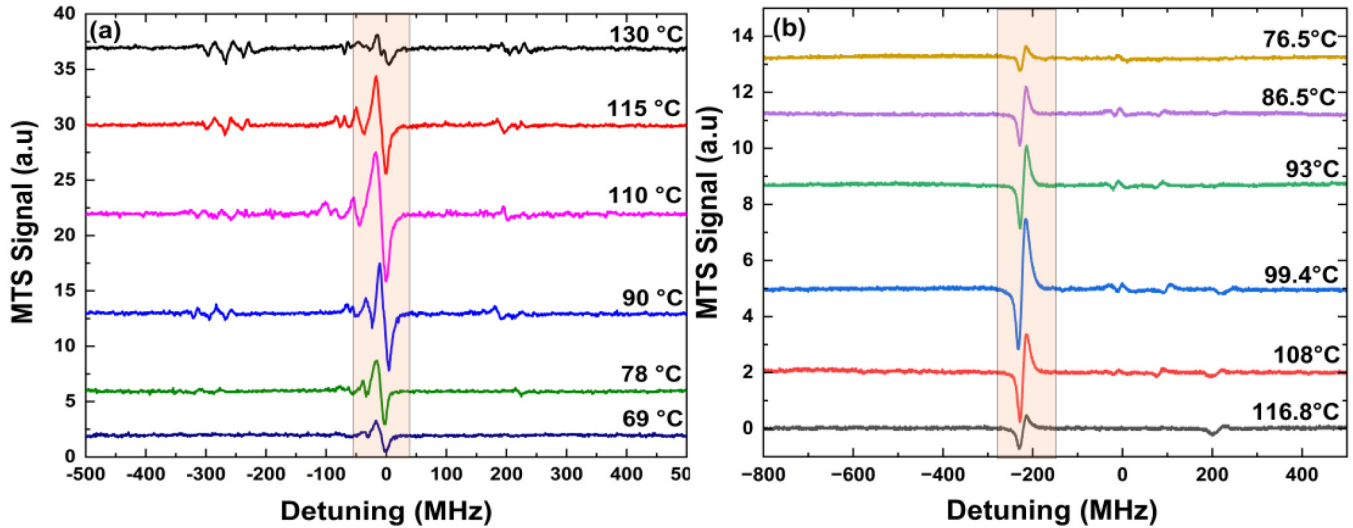


FIG. 5. (a) and (b) present the temperature-dependent MTS spectra as a function of detuning for the D1 and D2 transitions, respectively. The red faint color highlights the specific transition of interest for this study, emphasizing its behavior under varying temperature conditions. All the data are taken in the  $\sigma^+ - \sigma^+$  polarization configuration.

peak  $F = 2 \rightarrow F' = 3$ , compared to other transitions and crossover peaks. In the four polarization combinations, the lin  $\parallel$  lin configuration is bigger than the lin  $\perp$  lin configuration, which is opposite to the D1 transition. While in the case of the  $\sigma^+ - \sigma^-$  polarization configuration, the amplitude is lower than the  $\sigma^+ - \sigma^+$  configuration, which is similar to the D1 transition.

For simple understanding, if the pump laser is tuned to  $F_g = 2 \rightarrow F_e = 1$ , the magnetic sub-levels (i.e.,  $m_F$  states)  $|F_g = 2, m_F = 0, \pm 1\rangle \rightarrow |F_e = 1, m_F = 0, \pm 1\rangle$  spontaneously collapse to  $|F_g = 1, m_F = 0, \pm 1\rangle$ . For the lin  $\parallel$  lin arrangement, the transition  $|F_g = 1, m_F = 0\rangle \rightarrow |F_e = 1, m_F = 0\rangle$  is not allowed, and  $|F_g = 1, m_F = 0\rangle$  does not engage in the modulation transfer spectroscopic method. But for the lin  $\perp$  lin configuration, each of the magnetic sub-levels for  $F_g = 1$  contributes to the MTS spectrum. Therefore, we can expect the crossover amplitude in the lin  $\perp$  lin arrangement to be greater than the lin  $\parallel$  lin polarization arrangement, which agrees with our experimental results. If we tune the pump light to regulate  $F_g = 1 \rightarrow F_e = 1$ , then the crossover spectrum's amplitude in the lin  $\parallel$  lin configuration is greater than in the lin  $\perp$  lin polarization arrangement.

In the case of the circular polarization configuration, the pump beam polarization with  $\sigma^- (\sigma^+)$  populates all the atoms in  $|F_g = 2, m_F = -2\rangle$  ( $|F_g = 2, m_F = 2\rangle$ ). If the probe beam is tuned with  $\sigma^- (\sigma^+)$ , then the atoms will transition  $|F_g = 2, m_F = -2\rangle \rightarrow |F_e = 1, m_F = -1\rangle$  or  $|F_g = 2, m_F = 2\rangle \rightarrow |F_e = 1, m_F = 1\rangle$ , which is almost a closed transition and provides a large MTS spectrum. Similarly, if the probe beam polarization is  $\sigma^+ (\sigma^-)$ , then the transitions involved in the MTS spectrum are  $|F_g = 2, m_F = -2\rangle \rightarrow |F_e = 1, m_F = 1\rangle$  or  $|F_g = 2, m_F = 2\rangle \rightarrow |F_e = 1, m_F = -1\rangle$ , which is not a closed transition, and we get a smaller MTS spectrum, which greatly agrees with our experimental results.

In the case of the D2 line, the  $F = 2 \rightarrow F' = 3$  transition generates the maximum amplitude and slope of the MTS spectrum, compared to other transitions and crossover peaks. We have noticed the same kind of behavior while playing with the polarization. We have detected the maximum amplitude and slope of the MTS spectrum in the  $\sigma^+ - \sigma^+$  polarization configuration. But, we observed the amplitude and slope for the  $F = [1 \leftrightarrow 2] \rightarrow F' = 2$  crossover in the D1 line to be much higher than the  $F = 2 \rightarrow F' = 3$  transition in the D2 line. The four-wave mixing mechanism can interpret the MTS spectrum for the cycling transition. The atom population determines the amplitude and transition probability, which is known as branching ratios.<sup>25</sup> We can reveal that the FWM process is different in different polarization configurations, because different magnetic sublevels of the atoms are involved.

## B. Temperature dependence of D1 and D2 spectra

Next, we investigated the modulation transfer spectroscopy spectra of the D1 and D2 transitions at various temperatures to study their thermal dependence. Figure 5 illustrates the temperature-dependent behavior of the D1 and D2 spectra. The D1 spectrum is characterized by strong crossover resonances, a consequence of the small ground-state hyperfine splitting in potassium. These crossover features exhibit significant sensitivity to temperature, making the D1 transition particularly suitable for applications in atomic thermometry. This section explores the influence of temperature and the polarization of the pump and probe beams on the MTS spectrum.

In Fig. 5, the MTS spectrum is analyzed as a function of the potassium vapor cell temperature. For the D1 transition, the pump and probe beam intensities were maintained at  $36.75 \pm 0.06$  and  $22.05 \pm 0.01$  mW/cm<sup>2</sup>, respectively. For the D2 transition, the corresponding intensities were  $13.7 \pm 0.05$  mW/cm<sup>2</sup> (pump) and

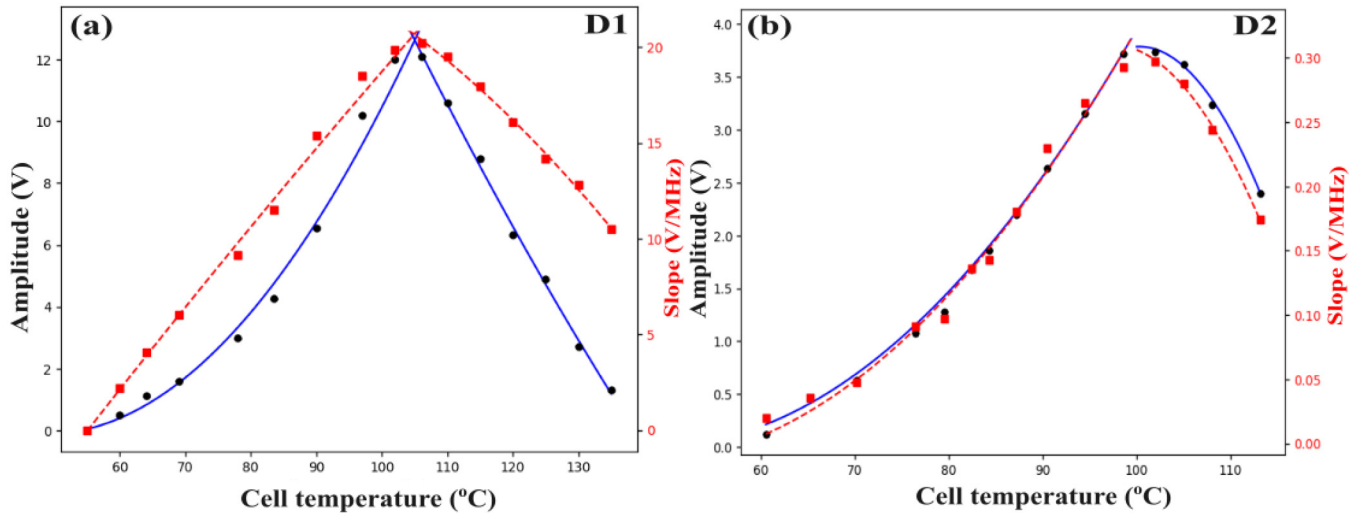


**FIG. 6.** Amplitude (V) as a function of cell temperature ( $^{\circ}\text{C}$ ) for different experimental conditions. The data, presented in tabular form, show the variation in amplitude across a temperature range of 70 to  $140^{\circ}\text{C}$ . Each row corresponds to specific measurements or configurations, providing insights into the temperature-dependent behavior of the system. This figure highlights trends in the amplitude response, aiding in the optimization of experimental parameters.

$7.38 \pm 0.01 \text{ mW}/\text{cm}^2$  (probe). The figure highlights the significant impact of temperature on the amplitude and slope of the MTS signal. For both transitions, the amplitude and slope initially increase sharply with temperature, reaching maxima at  $104 \pm 3^{\circ}\text{C}$  for the D1 transition and  $96 \pm 2^{\circ}\text{C}$  for the D2 transition. Beyond these temperatures, the signal amplitude and slope decrease dramatically. This behavior can be attributed to the interplay between atomic vapor density and optical pumping efficiency. At lower temperatures, the atomic vapor density is insufficient to produce a strong signal. As the temperature increases, the vapor density rises, leading to an enhancement in the MTS signal amplitude and slope. However, at higher temperatures, increased collisions between atom-atom and the atom-cell walls reduce the efficiency of optical pumping, causing the signal to diminish. This temperature-dependent response underscores the importance of optimizing the cell temperature for precise spectroscopic measurements. All measurements were conducted using the beam intensities mentioned earlier, with minimal time intervals between data points to ensure consistency and accuracy. For the D1 transition, the MTS spectrum reveals the  $F = [1 \leftrightarrow 2] \rightarrow F' = 2$  crossover transition, a feature that has been recently reported for  $^{39}\text{K}$ .<sup>5</sup> A similar crossover transition was observed in lithium MTS spectra,<sup>24</sup> where it was attributed to incoherent processes. While other modulated resonances and crossover peaks are present in the D1 spectrum, their amplitudes and slopes are significantly smaller compared to the dominant crossover feature, making the  $F = [1 \leftrightarrow 2] \rightarrow F' = 2$  transition the most prominent.

For the D2 transition, the MTS spectrum is primarily characterized by the  $F = 2 \rightarrow F' = 1, 2, 3$  transitions. Among these, the cycling transition  $F = 2 \rightarrow F' = 3$  dominates the spectrum, producing a strong and well-defined MTS signal. A qualitative comparison between the MTS and saturated absorption spectra reveals

an interesting observation: the zero crossings of the MTS signal are shifted to higher frequencies relative to the centers of the saturated absorption peaks. This frequency shift suggests that the MTS spectrum for the D2 line is predominantly generated by the  $F = 2 \rightarrow F' = 3$  transition, which is verified by trapping the atoms in the optical trap.<sup>20,26,27</sup>

From Fig. 6, we conclude that the optimal cell temperatures for modulation transfer spectroscopy (MTS) measurements are  $104 \pm 3^{\circ}\text{C}$  for the D1 transition and  $96 \pm 2^{\circ}\text{C}$  for the D2 transition in a 2 cm long potassium vapor cell. These temperature values correspond to the conditions that yield the maximum signal amplitude and slope in the MTS spectra. Notably, these optimal temperatures closely match those observed in conventional saturated absorption spectroscopy (SAS), reinforcing the validity of our measurements and highlighting the consistency and reliability of our experimental methodology. A comparison of the two transitions reveals distinct thermal behaviors. In contrast to the D1 transition, the D2 spectrum shows a relatively weaker dependence on temperature. This reduced sensitivity is attributed to the larger hyperfine splitting in the excited state of the D2 line, which effectively suppresses crossover resonances that are otherwise prominent in the D1 spectrum. Despite this, the D2 transition remains a viable probe for temperature monitoring, particularly at higher temperatures where the D1 crossover features become less distinct and harder to resolve.

To systematically quantify the system's temperature sensitivity, we employed a quadratic fitting model to analyze the variation in signal response. We defined sensitivity as the derivative of signal amplitude with respect to temperature:  $\text{Sensitivity} = \frac{dV}{dT} = 2aV - 2a_1V + c$ , where  $a$ ,  $a_1$ , and  $c$  are the empirical fitting coefficients obtained from our data and  $V$  represents the measured signal amplitude or slope.

25 August 2025 08:50:43

**TABLE I.** Temperature sensitivity of the amplitude and slope of the Doppler-free MTS signal for selected atomic transitions. The values are given with their respective uncertainties. The negative values denoted for decline of amplitude and slope with increasing temperature.

Transitions	Sens. <sub>SI</sub>	
	Sens. <sub>Ampl</sub> (mV/°C)	(mV/MHz °C)
D1 (F = [1↔2] → F' = 2)	8±0.4	1 ± 0.02
	-2.8 ± 0.3	-5.2 ± 0.04
D2 (F = 2 → F' = 3)	3 ± 0.03	0.24 ± 0.02
	- 16.6 ± 0.07	- 1.8 ± 0.06

Positive sensitivity values indicate a region where the signal amplitude and slope increase with temperature, reaching a peak at the optimal point, whereas negative values denote a subsequent decline as the system surpasses the optimal thermal condition.

The extracted sensitivity values for both the signal amplitude and slope are summarized in Table I. These results provide a quantitative framework for evaluating the thermal response of the MTS system and offer practical guidelines for optimizing spectroscopic measurements in potassium vapor cells.

These results not only enhance our understanding of the temperature-dependent behavior of MTS spectra but also provide practical guidelines for optimizing experimental conditions in precision spectroscopy and atomic thermometry applications.

## V. CONCLUSION

In this study, we have demonstrated the potential of modulation transfer spectroscopy for both laser frequency stabilization and atomic thermometry using the D<sub>1</sub> and D<sub>2</sub> transitions in naturally abundant potassium vapor. The strong crossover resonances observed in the D<sub>1</sub> spectrum, arising from the small ground-state hyperfine splitting, exhibit significant sensitivity to temperature variations, making the D<sub>1</sub> transition particularly suitable for precise temperature measurements. In contrast, the D<sub>2</sub> transition, with its larger hyperfine splitting, shows weaker temperature dependence but remains valuable for spectroscopic applications.<sup>26,27</sup>

Our systematic investigation of temperature-dependent MTS spectra revealed optimal operating temperatures of  $104 \pm 3$  °C for the D<sub>1</sub> transition and  $96 \pm 2$  °C for the D<sub>2</sub> transition in a 2 cm potassium vapor cell. These findings align closely with results from saturated absorption spectroscopy, validating the consistency and reliability of our experimental approach. Furthermore, we explored the influence of different polarization configurations on the MTS signals, identifying the circular polarization  $\sigma^+ - \sigma^+$  configuration as the most effective for producing distinct zero-crossing features, which are crucial for precision frequency stabilization and thermometry.

The temperature sensitivity of the MTS signals, quantified through linear fitting, provides a robust framework for understanding the thermal response of atomic transitions. This work not only enhances our understanding of the interplay between atomic vapor dynamics and resonant detuning but also offers practical guidelines for optimizing experimental conditions in precision spectroscopy

and atomic thermometry. Future work will focus on refining the temperature measurement technique, extending its applicability to other atomic species, and exploring the role of higher-order interactions in improving the accuracy of MTS-based thermometry.

## ACKNOWLEDGMENTS

The author gratefully acknowledges the support of the Photonics Laboratory at Tampere University and the Department of Physics at Durham University for providing essential infrastructure and collaborative support. The author extends his sincere thanks to Professor Simon Cornish for granting access to his laboratory facilities and for his valuable input throughout the project. The author also appreciates the efforts of the technical staff, whose expertise and assistance were crucial in the construction and optimization of the experimental setup. Furthermore, the author acknowledges the financial support provided by the Government of India, which made this research possible.

## AUTHOR DECLARATIONS

### Conflict of Interest

The author has no conflicts to disclose.

### Author Contributions

**Prosenjit Majumder:** Conceptualization (lead); Data curation (lead); Investigation (lead).

## DATA AVAILABILITY

The data that support the findings of this study are available from the corresponding author upon reasonable request.

## REFERENCES

- <sup>1</sup>W. D. Phillips, "Nobel lecture: Laser cooling and trapping of neutral atoms," *Rev. Mod. Phys.* **70**, 721–741 (1998).
- <sup>2</sup>D. McCarron, "Laser cooling and trapping molecules," *J. Phys. B At. Mol. Opt. Phys.* **51**, 212001 (2018).
- <sup>3</sup>N. Fitch and M. Tarbutt, "Laser-cooled molecules," in *Advances In Atomic, Molecular, and Optical Physics* (Elsevier, 2021), pp. 157–262.
- <sup>4</sup>W. Happer, "Optical pumping," *Rev. Mod. Phys.* **44**, 169–249 (1972).
- <sup>5</sup>A. D. Innes, P. Majumder, H. R. Noh, and S. L. Cornish, "Modulation transfer spectroscopy of the D1 transition of potassium: Theory and experiment," *J. Phys. B At. Mol. Opt. Phys.* **57**, 075401 (2024).
- <sup>6</sup>P. Majumder, H. Yadav, D. R. Tirupathi, K. Kant, S. Jain, P. Yadav, A. Ghosh, A. S. Deo, and D. Singh, "Advancing frequency locking: Modified FPGA-guided direct modulation spectroscopy for laser stabilization" (2023).
- <sup>7</sup>D. J. McCarron, S. A. King, and S. L. Cornish, "Modulation transfer spectroscopy in atomic rubidium," *Meas. Sci. Technol.* **19**, 105601 (2008).
- <sup>8</sup>H.-R. Noh, S. E. Park, L. Z. Li, J.-D. Park, and C.-H. Cho, "Modulation transfer spectroscopy for <sup>87</sup>Rb atoms: Theory and experiment," *Opt. Express* **19**, 23444–23452 (2011).
- <sup>9</sup>T. Preuschoff, M. Schlosser, and G. Birkel, "Optimization strategies for modulation transfer spectroscopy applied to laser stabilization," *Opt. Express* **26**, 24010 (2018).
- <sup>10</sup>J. Baek, S. Park, M.-H. Lee, H.-R. Noh, and G. Moon, "Polarization-selective four-wave mixing in a degenerate multi-level system," *Sci. Rep.* **14**, 5705 (2024).

- <sup>11</sup>L. Mudarikwa, K. Pahwa, and J. Goldwin, "Sub-Doppler modulation spectroscopy of potassium for laser stabilization," *J. Phys. B At. Mol. Opt. Phys.* **45**, 065002 (2012).
- <sup>12</sup>P. G. Pappas, M. M. Burns, D. D. Hinshelwood, M. S. Feld, and D. E. Murnick, "Saturation spectroscopy with laser optical pumping in atomic barium," *Phys. Rev. A* **21**, 1955–1968 (1980).
- <sup>13</sup>P. R. Berman and V. S. Malinovsky, *Principles of Laser Spectroscopy and Quantum Optics* (Princeton University Press, 2011).
- <sup>14</sup>S. J. Hale, W. J. Chaplin, G. R. Davies, and Y. P. Elsworth, "Modelling the response of potassium vapour in resonance scattering spectroscopy," *J. Phys. B At. Mol. Opt. Phys.* **53**, 085003 (2020).
- <sup>15</sup>W. T. Hicks, "Evaluation of vapor-pressure data for mercury, lithium, sodium, and potassium," *J. Chem. Phys.* **38**, 1873–1880 (1963).
- <sup>16</sup>W. Edmondson and A. C. Egerton, *Proc. R. Soc. London Ser. A* **113**, 520–533 (1927).
- <sup>17</sup>E. Arimondo, M. Inguscio, and P. Violino, "Experimental determinations of the hyperfine structure in the alkali atoms," *Rev. Mod. Phys.* **49**, 31–75 (1977).
- <sup>18</sup>S. Falke, E. Tiemann, C. Lisdat, H. Schnatz, and G. Grosche, "Transition frequencies of the *d* lines of <sup>39</sup>K, <sup>40</sup>K, and <sup>41</sup>K measured with a femtosecond laser frequency comb," *Phys. Rev. A* **74**, 032503 (2006).
- <sup>19</sup>L. Zhe Li, S. Eon Park, H.-R. Noh, J.-D. Park, and C.-H. Cho, "Modulation transfer spectroscopy for a two-level atomic system with a non-cycling transition," *J. Phys. Soc. Jpn.* **80**, 074301 (2011).
- <sup>20</sup>P. Majumder, "Towards the trapping of single potassium atoms in optical tweezers," Ph.D. thesis (Durham University, 2022).
- <sup>21</sup>S. Lee, J. Kang, S. Kim, J. Jeong, G. Moon, and H.-R. Noh, "Magnetic-field enhanced modulation transfer spectroscopy: Theory and experiment," *Opt. Express* **29**, 34770 (2021).
- <sup>22</sup>G.-W. Choi and H.-R. Noh, "Line shapes in sub-Doppler DAVLL in the <sup>87</sup>Rb-D2 line," *Opt. Commun.* **367**, 312–315 (2016).
- <sup>23</sup>D. J. McCarron, I. G. Hughes, P. Tierney, and S. L. Cornish, "A heated vapor cell unit for dichroic atomic vapor laser lock in atomic rubidium," *Rev. Sci. Instrum.* **78**, 093106 (2007).
- <sup>24</sup>D. Sun, C. Zhou, L. Zhou, J. Wang, and M. Zhan, "Modulation transfer spectroscopy in a lithium atomic vapor cell," *Opt. Express* **24**, 10649 (2016).
- <sup>25</sup>A. Lindgård and S. E. Nielsen, "Transition probabilities for the alkali isoelectronic sequences Li I, Na I, K I, Rb I, Cs I, Fr I," *At. Data Nucl. Data Tables* **19**, 533–633 (1977).
- <sup>26</sup>B. S. Marangoni, C. R. Menegatti, and L. G. Marcassa, "Loading a 39K crossed optical dipole trap from a magneto-optical trap," *J. Phys. B At. Mol. Opt. Phys.* **45**, 175301 (2012).
- <sup>27</sup>C. R. Menegatti, B. S. Marangoni, J. Tallant, and L. G. Marcassa, "Simultaneous loading of <sup>39</sup>K and Rb into a crossed dipole trap: Characterization and two-body losses," *Phys. Rev. A* **88**, 023411 (2013).